Settlements and angular distortions of shallow foundations on liquefiable soil

Anna Baris (anna.baris@unicas.it)
Universita degli Studi di Cassino e del Lazio Meridionale Dipartimento di Ingegneria Civile e Meccanica https://orcid.org/0000-0002-1346-9786
Giuseppe Modoni
Universita degli Studi di Cassino e del Lazio Meridionale Dipartimento di Ingegneria Civile e Meccanica
Luca Paolella
Universita degli Studi di Cassino e del Lazio Meridionale Dipartimento di Ingegneria Civile e Meccanica
Erminio Salvatore
Universita degli Studi di Cassino e del Lazio Meridionale Dipartimento di Ingegneria Civile e Meccanica
Rose Line Spacagna
Universita degli Studi di Cassino e del Lazio Meridionale Dipartimento di Ingegneria Civile e Meccanica

Research Article

Keywords: Liquefaction damage, settlement, angular distortion, artificial neural network, numerical analysis

Posted Date: May 6th, 2022

DOI: https://doi.org/10.21203/rs.3.rs-1553799/v1

Abstract

The huge impact caused by liquefaction during past earthquakes has raised the need for predictive formulas applicable at the large scale to forecast the movement in the foundation caused by the seismic liquefaction phenomenon in sands. A method herein developed with this aim to quantify angular distortion of framed low-rise buildings based on simple characterization of the seismic input, subsoil and structure. The analysis moves from past literature criteria introduced to quantify the vulnerability of buildings under static conditions and extends their applicability to liquefaction assessment integrating recent literature predictive formulas, parametric two-dimensional numerical analyses and artificial neural networks. Numerical calculation, performed for variable stratigraphic and mechanical characteristics of the subsoil, ground motion and equivalent flexural stiffness of the building, quantifies the role of each factor on the absolute settlement and angular distortion. Then the dependency on the different factors of the angular distortion is inferred with an artificial neural network (ANN), grouping parameters to limit the number of input variables and express results with charts that make prediction more accessible.

1. Introduction

Seismic liquefaction continuously stimulates the interest of the geotechnical community in promoting experimental, theoretical studies and field observations that clarify the factors ruling susceptibility of soil, triggering (e.g., Ishihara, 1996; Youd TL *et al.*, 2001; Seed *et al.*, 2003; Bray and Sancio, 2006; Boulanger and Idriss, 2014) and chained mechanisms (Iwasaki *et al.*, 1978; van Ballegooy *et al.*, 2014; Chiaradonna *et al.*, 2020; Cubrinovski *et al.*, 2017). For buildings and infrastructures, studies are oriented at predicting damage (Bird *et al.*, 2005; Bray & Macedo, 2017; Karamitros *et al.*, 2013; Bullock *et al.*, 2018; Castiglia *et al.*, 2020; Baris *et al.*, 2021) or at conceiving mitigative solutions (Flora *et al.*, 2021; Salvatore *et al.*, 2020), motivated by the concern of stakeholders for the huge economic and social impact of liquefaction recorded in past seismic events. An overall estimate is provided by Daniell *et al.* (2012) who disaggregated primary (shaking) and secondary causes (tsunami, fire, landslides, liquefaction, fault rupture, and other type losses) over a global record of nearly seven thousand earthquakes from 1900 to 2012. These authors found liquefaction responsible for about 2.2% of the direct economic losses, globally estimated in 2.24 trillion US dollars, this fraction becoming 3.6% when considering total losses, i.e. direct plus indirect damage. This relatively small percentage could misleadingly drive to underestimate the relevance of liquefaction, but the numerous examples occurred in urbanized systems prove that the physical damage together with the prolonged impracticability of buildings and infrastructures can be overwhelming, as it undermines the recovery of normal life conditions and may lead to the complete abandonment of the place (Macaulay *et al.*, 2009; CSAPEISLA, 2016). Literature reports plenty examples of destructive effects caused by liquefaction on urban arear (San Francisco 1960 - Youd and Hoose, 1978; Kobe 1995 - Chung, 1996; Kocaeli 1999 - Cetin *et al.*, 2002; Christchurch 2010–2011 - Cubrinovski *et al.*2011, Bray *et al.*2014, Paolella *et al.*, 2020; Urayasu 2011 - Yasuda *et al.*, 2012; Baris *et al.*, 2021; Emilia-Romagna 2012 - Fioravante *et al.*, 2013). This phenomenon is strongly ruled by the soil-foundation-structure interaction (Bray *et al.*, 2014). When liquefaction occurs at some depth, the reduced dynamic impedance of the softened stratum diminishes the acceleration on the superstructure. Evidence of liquefaction damaged buildings exhibiting limited shaking effects suggest that a sort of isolation may take place at the foundation level, but proofs exist as well of buildings damaged by both shaking and liquefaction (e.g. Bird and Bommer, 2004). Fully coupled analyses of liquefaction and shaking are rather complex and require a very accurate definition of the input variables, difficult to achieve when performing serial analyses like in large scale assessment. Bird *et al.* (2006) proposes a simpler solution that decouples and recombines effects of shaking and liquefaction for a prescribed event. First compulsory step is the definition of a demand variable, i.e. the most expressive quantity that characterizes physical damage. Foundation movement is classically subdivided into the following components: mean settlement, rigid rotation and angular distortion. While rotation is of paramount importance for high rise buildings and towers, prEN 1997-1 (2004) and Poulos *et al.* (2001) converge on identifying the angular distortion as the paramount demand variable for low-rise buildings (1–3 stories, Fotopoulou *et al.*, 2018), fixing thresholds equal to 1/500, 1/300 or 1/150 for respectively light, visible cracking, and structural damage of framed buildings. A similar assumption is also made by studies focused on the effect of static loading on buildings (e.g. Skempton and MacDonald, 1956; Bjerrum, 1963; Meyerhof, 1953; Burland and Wroth, 1974; Burland *et al.*, 1977; Wahls 1981). Boscardin and Cording (1989) studied the effects of excavation and defined the damage level as a function of angular distortion and horizontal tensile strain, the two quantities related to each other for the different source of movement. This step is simplified by Grant *et al.*(1974) that propose to statistically estimate angular distortion as the upper bound from a relation with absolute settlements measured on buildings founded on cohesive or cohesionless soils with rafts, strips or isolated footings.

For liquefaction assessment of low-rise buildings, Bird *et al.* (2006) distinguishes the case of rigid from flexible foundation, with absolute settlements being the principal damage factor for the former, differential settlement for the latter case. In this circumstance, differential settlements induced by liquefaction on framed buildings cause a drift of columns that the authors propose to cumulate to that produced by shaking. The differential settlement is also adopted as demand variable by Fotopoulou *et al.* (2018) in their probabilistic definition of vulnerability for low-grade structures. In general, the structural damage induced by foundation movements on a building depends on the stiffness and fragility of the structure-foundation system, these factors connected with the typology, extension, and height of the building. A continuous transition, rather than a net separation between rigid and flexible structures, would better describe the variety of possible structural typologies.

For liquefaction, several methods are proposed to predict absolute settlements. The state-of-the-art practice for this evaluation largely relies on empirical procedures developed to estimate post-liquefaction, one dimensional consolidation settlement in free-field condition (e.g., Tokimatsu and Seed, 1987; Ishihara and Yoshimine, 1992). According to Ishii and Tokimatsu (1988), this assumption can be reasonably accepted only if the width of the foundation is at least twice or three times larger than the thickness of the liquefiable soil layer. However, the main limitation of these empirical procedures is that none of them considers the soil-structure interaction and the resulting complex mechanisms, for example the SSI-induced building ratcheting during earthquake loading (Dashti and Bray, 2013). Based on the results of numerical analyses and attributing liquefaction induced settlements to the seismic

excitation characteristics and the post-shaking degraded static factor of safety, Karamitros *et al.* (2013) provide a simplified analytical formula for the estimation of absolute settlement of strip and rectangular footings with a clay crust. Such settlement is associated with a "sliding-block" type of punching failure through the clay crust and within the liquefied sand layer. Bray and Macedo (2017) performed a large number of parametric numerical analyses and proposed to express the total settlement as a sum of three contributions respectively induced by shear, volume deformation and sand ejecta; in particular, the shear-induced rate is related to several properties, including the unitary contact pressure on the foundation, the thickness of the liquefiable layer and the lower planimetric dimension of the building footprint and the cumulative absolute velocity (Campbell & Bozorgnia, 2011). Performing a rich and various parametric numerical, fully coupled three-dimensional analyses of the soil–structure interaction, Bullock *et al.* (2018) define a relation to predict the statistical distribution of settlements for shallow-founded structures on liquefiable soil induced by volumetric and distortional strains. This formula has the advantage of capturing the role of most soil, ground motion and building properties.

The present paper summarizes the above concepts into an automated tool to forecast the expected angular distortion in foundation, extensively applicable to framed low-rise buildings on shallow foundations. To this aim, a large number of two-dimensional coupled numerical analyses are performed, parametrically varying the stratigraphic and mechanical conditions of the subsoil, the ground motion characteristics and the equivalent structural properties of the building. The analysis, focused on the angular distortion, attempts to infer a relation with the relevant properties by means of artificial neural networks.

2. Numerical Analysis

2.1 Definition of the model

The implemented numerical model (Figure 1) intends to represent the most generic conditions with a Finite Difference code (FLAC v8, Itasca, 2016), exploiting the flexibility and available library of advanced constitutive models provided by this tool. The calculation setup has been validated assigning specific seismic, subsoil and building conditions of a known case study where liquefaction was carefully surveyed. The adopted two-dimensional layout consists of three horizontal layers developed on a width of 40 meters and a total depth of 20 meters, with an upper low-permeability cap (Layer #1), an intermediate liquefiable layer (Layer #2) and a lower base clay (Layer #3). The typical calculation mesh consists of 13,980 rectangular elements of 0.8m width and variable heights (0.5 m for the above and below layers, 0.4 for the liquefiable layer), these dimensions chosen after the suggestion of Kuhleimeyer & Lysmer (1973), who found that propagation of seismic waves in continuum media can be simulated with sufficient accuracy if the element's dimension is smaller than 1/10 of the minimum propagating wavelength. The stress-strain response of the liquefiable soil has been simulated with *PM4Sand* Version 3.1 (Boulanger and Ziotopoulou, 2017) chosen thanks to its capability to capture the cyclic behavior of saturated sand. It represents an evolution of the Dafalias and Manzari (2004) formulation, being a stress-ratio controlled, critical state compatible, bounding surface plasticity model developed primarily for earthquake engineering applications (Boulanger and Ziotopoulou, 2015). The stress-strain response of the shallow and deepest layers is simulated using Mohr-Coulomb hysteretic model, considering the stress state induced into the subsoil by the above building. Luque and Bray (2015) and Luque and Bray (2017) showed that the primary aspects of the dynamic response of a 3D system in terms of liquefaction-induced building settlement can be captured in 2D analyses by using tributary mass and stiffness with the primary goals being to capture the mass and stiffness. The superstructure is modeled with an equivalent beam characterized with a flexural stiffness (EI) and a contact pressure (q). The EI modulus summarizes the bending stiffness of the building-foundation system. For framed buildings it can be computed dividing the sum of stiffnesses of all parallel longitudinal frames by the transversal extension of the building. A lower bound stiffness of frames can be computed neglecting the upper decks and considering the transverse section of the foundation element only (Mazzolani, 1967), nil in case of isolated footings. Alternatively, a more realistic estimate can be obtained adding the bending moments of the upper decks, computing the moments of inertia of transverse sections with reference to the center axis of each deck (Sherif and Koenig, 1975).

The contact pressure *q* summarizes the contribution of all building floors and can be computed multiplying the number of floors times the overall unit load, i.e. the load per unit area including the self-weight of structural and non-structural elements and the accidental loads.

2.2 Calibration and validation

The prototype model has been firstly validated with the back-analysis of a building located in the Municipality of Terre del Reno, whose data are extracted from the Emilia-Romagna Regional database. The building consists of a two storeys masonry building with a rectangular layout (length 13.10 m, width 11.10 m) founded on a shallow slab of poor structural characteristics. The liquefaction induced by the May 20th earthquake (M_w=6.1) caused significant differential settlements in the East-West direction, with an absolute settlement of 35 cm on the West side and 5 cm on the East side (Figure 2.b). Being the epicenter located about 15 km far from the building**, at a depth approximately equal to 10 km below the ground level** (Luzi *et al.*, 2019), **the acceleration time history assigned for the back analysis (Figure 2.c) has been computed transferring to the considered site the signal recorded at the nearest seismic station (Mirandola, from** the ITACA seismic catalogue**) with the procedure suggested by Sinatra & Foti (2015). These authors propose to deconvolve the acceleration time history recorded at the station to recover the signal the seismic bedrock, then apply the attenuation law proposed by** Bindi *et al.* (2011) to move from the station to the studied site, then perform a local seismic response analysis to obtain the input at the model's base. In the analysis, the deeper subsoil model has been taken from Fioravante *et al.* (2013), while the top subsoil stratigraphy has been reconstructed considering various CPTU tests performed in the closest area around the building (Figure 2.a).

The physical properties for the three strata have been derived from Fioravante *et al.* (2013), while permeability, friction angle (ϕ), cohesion (c) and undrained shear strength (c_u) of the fine-grained soils are taken from Sinatra and Foti (2015). For the upper and lower layers, the experimental stiffness decay and damping curves have been derived from Fioravante *et al.* (2013) and their calibration has been performed simulating the cyclic simple shear tests with the adopted numerical model (Figure 3). Finally, the effective strength values and the large strain stiffness parameters have been taken from the literature (Itasca Consulting Group, Inc., 2016).

The *PM4Sand* model for the intermediate layer (#2) has been calibrated setting twenty one parameters with the default values recommended by Boulanger and Ziotopoulou (2017) and finding the remaining three (i.e. sand's apparent relative density Dr, shear modulus coefficient G_o, and contraction rate parameter h_{po}) reproducing with the numerical code (FLAC v8, Itasca, 2016) the cyclic undrained behavior of the liquefiable sandy layer seen on four triaxial undrained cyclic tests performed by Facciorusso *et al.* (2016) Figure 4.a, 4.b and 4.c. The complete list of models and parameters for the three layers is given in (Table 1).

The building has been simulated with an elastic body of given width (B=12m), flexural stiffness (EI=60 MN*m) and contact pressure (q=50 kPa). The performed analysis returned a significant rotation of the building with a final vertical displacement at the west corner of 37 cm and at the east side corner of about 4 cm. The similarity between computed and observed settlements confirms that the adopted numerical tool can be reliably adopted for simulating the effects of liquefaction upon general conditions as accomplished in the following parametric study.

Table 1. Subsoil parameters assigned in the calculation.

Stratum	Model	n	γ_{nat} (kN/m^3)	Permeability	φ' (°)	C' (kPa)	Cu (kPa)	K (Mpa)	G (Mpa)	c0	c1	Dr	G0	hp0	nb	Nd
Silty cap	Mohr-Coulomb	0.5	16.5	1.00E-07	28	2	34	2.67	1.6	-3	0.2	/	/	/	/	/
Sands	PM4Sand	0.5	18.5	7.00E-06	33	0	/	16.7	10	/	/	0.4	507	20	0.5	0.1
Clays	Mohr-Coulomb	0.4	18	6.00E-08	20	8	45	0.67	0.4	-2	0.2	/	/	/	/	/

2.3 Parametric study

The physical, mechanical and geometrical factors varied in the parametric analysis have been chosen following Karimi *et al.* (2018) who observed the mean permanent settlement of the building is affected by respectively contact pressure, seismic input, thickness, relative density and depth of the liquefiable layer, but also by the presence of a low-permeability cap. These parameters have thus been varied in the model as summarized in Table 2, positioning the water table at the ground level for all calculations. The structure-foundation system has been modeled with an equivalent plate characterized by width (B) and flexural stiffness modulus (EI). (see Table 2). In addition a set of six numerical analysis has been performed to evaluate relevance of the structure's inertial mass, simulating height/width ratio (H/B) ranging between 0.5 and 1.5.

Finally, considering the fundamental role played by the earthquake magnitude, four waveforms have been applied in the analysis, extracting them from the PEER Strong Ground Motion Databases. The velocity time history of these events, chosen thanks to their largely different Arias intensity (Table 3), have been scaled by three amplitude factors, respectively 0.7, 1.0 and 1.6 in order to introduce the role of earthquake intensity in the analysis. Combining the seismic input with the parameters reported in Table 2, about 320 analyses have been carried out.

The typical output of calculation consists of the displacements profile below the foundation (Figure 5) from which the following characteristic variables are extracted:

- maximum, minimum and mean settlement: $w_{Max,}$ w_{min} and w_{av};

- angular distortion: β;

- horizontal deformation: e_h.

Table 2. Parameters for sensitivity analyses

Parameter	Description	Range of variation
Hc	Layer #1 (non-liquefiable crust) thickness (m)	2 to 6 m
HL	Layer #2 (liquefiable layer) thickness (m)	4 to 12 m
Hb	Layer #3 (lower clay) thickness (m)	20 m-HL-Hc
Dr	Relative density of the liquefiable layer (%)	20 to 60%
s_u	Undrained shear strength of crust and lower clay (kPa)	25 to 100 kPa
B	Foundation base width (m)	10 to 30 m
Q	Contact pressure at the building foundation (kPa)	25 to 100 kPa
EI	Equivalent stiffness of the building foundation system (MN*m)	0 to 260 MN*m
PGV	Peak ground velocity (m/s)	0.23 to 0.63 m/s

Table 3. Selected seismic input.

Earthquake	PGV (m/s)	Ia (m/s)
Emilia-Romagna	0.33	0.64
Northridge	0.42	4.5
Imperial Valley	0.47	1.6
Northridge	0.63	2.8

2.3 Sensitivity study

A sensitivity study has been initially performed to understand the relative influence of the varied parameters on the kinematic variables defined in Figure 5. Firstly, the relation between mean and maximum settlements (w_{av} and w_{MAX}) has been investigated (Figure 6) as their equivalence is needed for the following analyses where their outputs are alternatively related to the angular distortion of the building-foundation system. Figure 6 shows a proportionality between these two variables, being the ratio w_{av}/w_{max} equal on average to 0.84, with minimum and maximum values equal to respectively 0.73 and 0.98.

The results of calculation are then summarized looking at the dependency of maximum, differential settlement, and angular distortion (respectively w_{MAX}, δ and β) on each of the parameters varied in the analysis. Figures 7 to 12 show sample results obtained assigning the seismic input of Emilia Romagna scaled for the different amplifying factors. Figures 7 and 8 point out the influence of the upper impervious crust characterized with thickness (H_C) and undrained shear strength (s_u). All curves show the positive role of both parameters on all the considered components of the foundation movement, attenuation rates being more remarkable for the stronger seismic events. Settlements reduce almost linearly within the considered thickness range ($H_c \leq 6$ m) for the higher seismic intensities (f=1.0 and 1.6), while reduction is smoother for the lower intensity earthquake (f=0.7) (Figure 7); attenuation rate is very high for undrained shear strength s_u increasing up to 50 kPa, then drops progressively for increasing s_u (up to 100 kPa and more) (Figure 8). The two plot sets reveal that, despite preventing the excess pore pressure exhaust, the impervious crust contributes significantly with its strength to limit the liquefaction effects on buildings.

Figures 9 and 10 show the influence of the liquefiable layer. The settlements and deformation increase rather continuously with thickness (H_L), being rates dependent on the earthquake intensity (Figure 9). On the contrary, variation with soil density is sharper, effects being critical for low density material (D_r=20%) where w_{MAX} reaches values as high as 2.5m (for f=1.6), then reduces rapidly for D_r=40%, moreover for D_r=60%.

Finally, Figures 11 and 12 summarize the effect of the building-foundation system, characterized by length B and flexural stiffness EI. Width produces a noticeable reduction on the absolute settlements throughout the considered variation (Figure 11.a), less evident on the differential component (Figure 11.b and c). On the other hand, flexural stiffness EI produces a continuous reduction on the differential settlements and angular distortion (Figure 12. b and c) but has negligible effects on the absolute settlements (Figure 12.a).

2.3.1 Role of Superstructure Inertia

Considering the limited relevance of the structure's inertial mass and of the height/width ratio seen by Karimi *et al.* (2018) and willing to limit the analysis to low-rise buildings, the structure-foundation system has been modeled with an equivalent plate so that inertia effects from the superstructure were avoided. In order to investigate the consistency of this assumption, six numerical simulations have been performed modelling the framed superstructure, considering several height/width ratios (H/B). The equivalent-linear-perfectly-plastic response of structural components has been reproduced through beam elements that can sustain axial force, shear force, and bending moment. The effect of this simplification is presented in terms of ratio between

foundation movements computed with the basic analysis and the corresponding results of the parametric analyses with superstructure inertia (ρ). In particular, Figure 13 shows a negligible effect of the superstructure inertia on the predicted response, characterized by a variation ranging between -4% and +7%, for the examined cases. This finding is comparable with Karamitros *et al.* (2013), who observed a deviation of predictions less than ±5% and confirmed by field evidence. For instance, Yoshida et al. (2001) examined building behavior in Adapazari during the 1999 Kocaeli earthquake in Turkey and noted that buildings with a liquefaction induced settlements and tilts, did not suffer severe inertia-induced structural damage, as opposed to numerous buildings in the non-liquefied areas of the city, which totally or partially collapsed because of structural system failure. Karamitros *et al.* (2013) ascertained that these results are justifiable by two mechanisms acting as natural seismic isolation and minimizing the inertial forces developing on the superstructure as well as the associated horizontal shear forces and overturning moments applied to the foundation. The first mechanism is related to the sand stiffness degradation and its considerable decrease of the system's natural frequency, thus deamplifying the applied dynamic excitation. Furthermore, liquefaction also activates a failure mechanism, which further inhibits the input motion from propagating to the footing.

3. Prediction Of Settlements With The Bullock (2018) Formula

One main advantage of settlement prediction formulas consists in the possibility of massively estimating the performance of buildings distributed over a territory, which is one main step of risk assessment. With this aim, the recent literature proposes a variety of formulas to predict liquefaction induced settlements based on the main characteristics of the phenomenon, i.e. seismic input, subsoil properties and foundation bearing pressure (Dashti and Bray, 2013; Karamitros *et al.*, 2013; Bray and Macedo, 2017; Bullock *et al.*, 2018). Among them, the physics-informed semi-empirical probabilistic formula proposed by Bullock *et al.* (2018) is the last and probably the most comprehensive. The method, calibrated with the results of a 3D fully coupled numerical parametric study and validated with a database of field observations and centrifuge experiments, estimates the expected mean foundation settlement for a given set of input parameters. In this study, it has been applied to each condition analyzed with the above numerical calculation, using the spreadsheet provided by the authors (https://shidehdashti.com/geotech-links/) that requires the input of parameters listed in Table 4.

Table 4 Input parameters for the application of Bullock *et al.* (2018) semi-empirical formula

IP	Description	U.M
	Cumulative absolute velocity	cm/s
M_w	Moment magnitude of the earthquake	M_w
Rrup	Distance to rupture	km
H	Focal depth	km
Nst	Number of floors	-
q	contact pressure of the foundation	kPa
B	Foundation width	M
D_f	Foundation embedment depth	M
H_L	Thickness of the liquefaction-susceptible layer	M
D_L	Depth from the foundation base to the center of the liquefaction-susceptible layer	M
H_C	Non-susceptible crust thickness	M
q_{c1N}	CPT normalized cone tip resistance of the liquefaction-susceptible layer	-

The cumulative absolute velocity ( ) has been computed for each combination of seismic event (Table 3) and scaling factor, implementing the equation proposed by Bullock *et al.* (2017). Analogously, foundation contact pressure (q), width (B), depth of embedment (D_f), thickness of the non-susceptible crust (H_C) and liquefaction-susceptible layer (H_L), depth from the foundation base to the center of the liquefaction-susceptible layer (D_L) have been set equal to those given in the numerical calculation. The number of storeys (N_{st}) has been derived as a function of the bearing contact pressure, considering a ratio $q/N_{st}\approx 25$ kPa. Finally, the mean CPT normalized cone tip resistance (q_{c1N}) of the liquefiable sandy layer has been computed with the equation proposed by Boulanger & Idriss (2014), as function of the relative density (D_r):

$$q_{c1N} = 0.9\left(\frac{\frac{D_r}{100}+1.063}{0.465}\right)^{3.788} \quad (2)$$

The Bullock *et al.* (2018) method provides a cumulated probability curve of settlements having Log-normal distribution and standard deviation σ_{ln} equal to 0.67, these properties derived comparing the computed settlement with those observed from case history and centrifuge experiments. Finally, the mean settlement derived from the numerical calculation has been compared with the median value computed with the Bullock *et al.* (2018) formula into a one to one plot. The values reported in the bi-logarithmic plane of Figure 14 show a linear inference line (black continuous) with a regression coefficient

approximately equal to one (1.067) and a correlation coefficient (R^2) equal to 0.90 that confirm a reasonably good fit. It is worth observing that all points in the plot but few fall in the area formed by 16^{th} and 84^{th} percentile of the probability distribution, most of them positioning near the interpolating line. This result confirms a good predictive performance of the formula, similar to that noticed in their original work by Bullock *et al.* (2018).

4. Angular Distortion

The analysis of the angular distortion has been carried out looking at two classical studies on this subject for static loading, produced by Boscardin and Cording (1989) and Grant *et al.*(1974). The former authors proposed a vulnerability criterion applicable to brick bearing wall and small framed structures subjected to various underground events, from excavation to self-weight induced deformation, summarized in Fig. 15. This study focuses on the combination of angular distortion and horizontal strain at the foundation level, finding that the relative composition of these two kinematic components is dictated by the disturbing factor. In particular, underground excavation tends to produce larger horizontal strains compared with foundation loading, while angular distortion is predominant in the latter case. The two quantities, computed for each simulation of the present parametric study, give an alignment of dots in Fig. 15 along the line characteristic of self weight building settlements. This outcome implies that foundation movements occur with the same pattern, whether they are caused by static loading or liquefaction, being a possible explanation that subsoil deformation occurs at relatively shallow depths in both cases.

Another interesting result is obtained reporting angular distortion and maximum settlement obtained from each numerical calculation on the bi-logarithmic plot of Fig. 16, in analogy with the analysis performed by Grant *et al.*(1974). These authors collected observation on buildings founded on cohesive or cohesionless soils with shallow isolated or continuous footings and inferred an envelope curve for all monitoring data given by the following equation:

$$\beta_{MAX} = 7.8 \bullet 10^{-4} \bullet w_{MAX}$$

3

Interestingly, this curve reported with a continuous black line in Fig. 16 represents the upper bound also for the angular distortion computed in the present study. More particularly, this line interpolates quite closely the results obtained for nil bending stiffness while, for increasing EI values the angular distortion corresponding to the same maximum settlement tends progressively to diminish, consistently with the previous observation of Fig. 12.c. This evidence highlights once more that, despite reaching different absolute values, liquefaction induced settlements on low-rise buildings possess similar characteristics as those induced by static loading. This outcome, together with observation of Fig. 15, suggests possibility of adopting the same criteria used for static loading in the vulnerability assessment against liquefaction, i.e. assuming angular distortion as the demand variable for fragility and relating it to the maximum absolute settlements. This strategy implies predicting absolute settlements and relating them with angular distortion with simultaneously fast and reliable tools, useful for the risk assessment analysis on large territorial entities (e.g. urban systems).

5. Angular Distortion Predicted With Artificial Neural Network

Starting from the above consideration, angular distortion is adopted as engineering demand parameter for the vulnerability scrutiny of framed low-rise buildings and the availability of rapid tools for its estimate facilitates application to urban assets. With this goal in mind, the trends shown in the examples of Figs. 7–12 have been systematically interpreted with an analysis of variance (ANOVA, Fisher, 1918), determining the mutual influence of variables and separating those factors possessing a statistical relevance from others producing limited or random effects. Thereafter the relation between angular distortion and these variables has been sought training an artificial neural network, this tool preferred to the classical inference with mathematical functions thanks to its higher flexibility. Additionally, a minimum set of variables has been identified, grouping factors as much as possible, to render prediction more practical, e.g. in the form of graphical plots. After several trials, the median settlement computed with the Bullock *et al.*(2018) method, thickness and undrained shear strength of the crustal cap, bending stiffness of the building-foundation system have been identified as those compromising the lowest number of variables with an acceptable accuracy of prediction (see Table 5). Among them, the median settlement computed with the Bullock *et al.*(2018) method has the virtue of including most of the relevant factors (see Table 4) and provides a good estimate of the mean settlements (Fig. 13). This variable has been selected to group most of the factors also considering the dependency of angular distortion on the maximum settlement seen in Fig. 16 and the relation between mean and maximum settlement seen in Fig. 6. The remaining variables (H_c, s_u and EI) have been chosen because the one-way ANOVA test gave a significant outcome, i.e. indicated a statistical significance of the relation between the selected variables and angular distortion. The p-value from this test measures the probability that a relation could be of random nature, i.e. p-value tending to zero means a greater statistical significance of the observed relation. The very low p-values computed for the assumed variables (Table 5), all lower than the suggested threshold ($\alpha = 0.05$), confirm the reliability of relations.

Table 5
ANOVA test showing the statistical significance of the relation between variables and angular distortion.

Parameter	F	Significance value (α = 0.05)
EI (MN*m)	74.3	9.97E-25
Hc (m)	18.0	5.90E-25
s_u (kPa)	3.9	4.05E-07
$w_{Bullock}$ (m)	48.4	7.37E-20

These variables have thus been assigned as input of an Artificial Neural Network (ANN), trained with the output of numerical calculation and used to predict angular distortion in general cases (Fig. 17.a). The ANN is a mathematical model that replicates the brain functioning, being composed of interconnected neurons (McCulloch and Pitts, 1943). The one herein proposed is a two-layer feed-forward network with sigmoid hidden neurons and linear output neurons, in which information moves only in one direction from the input nodes through the hidden nodes to the output nodes, avoiding loops or recursive programming. In this study, architecture has been chosen as the best performing one among several attempts. The Levenberg-Marquardt backpropagation algorithm has then been used for training as it minimizes the sum of squares of nonlinear functions. The developed network has 10 hidden layers and the fractions of the dataset used for training, validation and testing are respectively equal to 70%, 15%, 15%.

The prediction, evaluated in terms of mean squared error MSE = $5.98*10^{-6}$ (Fig. 17.b), reveals a good performance over the whole investigated range. The statistical analysis of error shows (Fig. 17.c) a symmetric distribution well approximated with a gaussian probability density function (PDF(err)) having zero mean and standard deviation s(err) = 0.0007.

The proposed tool can be downloaded at the LAGGS - Geotechnics, Geology And Roads Laboratory website with the recommendation that prediction is reliable for values of the input variables included in the investigated range, i.e. $w_{Bullock} \leq 0.3$ m, EI ≤ 260 MN*m, $H_c \leq 6$ m and $s_u \leq 150$ kPa. An example of ANN outcome is provided in Fig. 18, where angular distortion b is plotted as function of median settlement $w_{Bullock}$ for selected values of flexural stiffness (EI equal to 0, 65 and 269 MN*m), undrained shear strength (s_u equal to 50 and 100 kPa) and crust thickness (H_c equal to 2, 4 and 6 m). The plots show the predominant role of equivalent bending stiffness of the building-foundation system, and the less relevant but still appreciable role of the upper crust layer.

Conclusion

The evidence of numerical calculation carried out in the present work shows that framed low-rise buildings, here schematized with a beam of given bending stiffness, present liquefaction induced settlements similar in their pattern to those induced by static loading. The angular distortion b has proven to be the predominant deformation component, while horizontal strain at the foundation level is negligible. Angular distortion increases with absolute settlement, the relation being strongly dictated by the equivalent building-foundation stiffness and b values being enveloped by the upper bound function experimentally observed by Grant *et al.*(1989). A procedure based on expert systems (an Artificial Neural Network) has thus been proposed to quantify b as function of the fundamental characteristics of earthquake, building and subsoil. For the sake of simplicity, the number of input variables has been minimized grouping most variables into the median settlement estimated with a semi-empirical method recently proposed by Bullock et al (2018), this method proving to replicate quite well the mean settlements obtained from the numerical calculation. The other considered input variables, i.e. the bending stiffness of the building-foundation stiffness, thickness and undrained shear strength of the crust layer have been selected considering their statistical relevance on b. With the adopted simplification, b can be computed either with a tool or with plots. Estimate has proven to be quite accurate, being the errors normally distributed with a standard deviation equal to s(err) = 0.0007.

A detailed analysis of results reveals the fundamental role of building-foundation bending stiffness, in accordance with Bird *et al.*(2006) who distinguished the case of rigid from flexible foundation, absolute settlements being the principal damage factor for the former, differential settlement for the latter type. Additionally, a positive contribution is given by the presence of an upper non-liquefiable crust, as also stated in the methods proposed by Karamitros *et al.* (2013).

References

1. Baris, A., Spacagna, R.L., Paolella, L., Koseki, J., Modoni, G. (2021). Liquefaction fragility of sewer pipes derived from the case study of Urayasu (Japan). *Bull Earthquake Eng* 19, 3963–3986. https://doi.org/10.1007/s10518-020-00957-2
2. Bindi, D., Pacor, F., Luzi, L., Puglia, R., Massa, M., Ameri, G., and Paolucci, R. (2011). Ground motion prediction equations derived from the Italian strong motion database. Bulletin of Earthquake Engineering, 9(6), 1899–1920.
3. Bird, J., Bommer, J. (2004). Earthquake losses due to ground failure. Engineering Geology. 10.1016/j.enggeo.2004.05.006
4. Bird, J. F., Crowley, H., Pinho, R., & Bommer, J. J. (2005). Assessment of building response to liquefaction-induced differential ground deformation. Bulletin of the New Zealand Society for Earthquake Engineering, 38(4), 215–234. https://doi.org/10.5459/bnzsee.38.4.215-234

5. Bird J, Bommer J, Crowley H, Pinho R (2006) Modelling liquefaction-induced building damage in earthquake loss estimation. Soil Dyn Earthq Eng 26(2006):15–30
6. Bjerrum, L. (1963). "Discussion session IV." Proc, European Conf. on Soil Mech. and Found. Engr., Wiesbaden, Germany, II, 135–137.
7. Boscardin, M.D. & Cording, E.J. (1989). Building response to excavation-induced settlement. Jn. Geotech. Eng., ASCE, 115(1): 1–21.
8. Boulanger, R.; Idriss, I. (2014). CPT and SPT Based Liquefaction Triggering Procedures; Report No. UCD/CGM-14/01; Center for Geotechnical Modeling, Department of Civil and Environmental Engineering, University of California:Davis, CA, USA, 2014.
9. Boulanger, R.W., and Ziotopoulou, K. (2015). PM4Sand (Version 3): A Sand Plasticity Model for Earthquake Engineering Applications Report No. UCD/CGM-15/01, Center for Geotechnical Modeling, Department of Civil and Environmental Engineering, University of California, Davis, CA, March, 114 pp.
10. Boulanger, R.W., and Ziotopoulou, K. (2017). "PM4Sand (version 3.1): A sand plasticity model for earthquake engineering applications." Report No. UCD/CGM-17/01, Center for Geotechnical Modeling, Department of Civil and Environmental Engineering, University of California, Davis, CA, March, 114 pp.
11. Bray, J., M. Cubrinovski, J. Zupan, and M. Taylor. (2014). "Liquefaction effects on buildings in the central business district of Christchurch." Earthquake Spectra 30 (1): 85–109. https://doi.org/10.1193 /022113EQS043M.
12. Bray J, Dashti S. (2014). Liquefaction-induced building movements. B Earthq Eng 2014; 12:1129–56.
13. Bray, J. & Macedo, J., (2017). 6th Ishihara lecture: "Simplified procedure for estimating liquefaction-induced building settlement". Soil Dynamics Earthquake Eng 102, 215–231.
14. Bray, J. & Sancio, R. (2006). Assessment of the Liquefaction Susceptibility of Fine-Grained Soils, Journal of Geotechnical and Geoenvironmental Engineering - J GEOTECH GEOENVIRON ENG, Vol. 132. 10.1061/(ASCE)1090 – 0241(2006)132:9(1165)
15. Bullock, Z., Dashti, S., Liel, A., Porter, K., Karimi, Z. & Bradley, B. (2017). Ground motion prediction equations for arias intensity, cumulative absolute velocity, and peak incremental ground velocity for rock sites in different tectonic environments. Bulletin of the Seismological Society of America 107(5), 2293–2309.
16. Bullock, Z., Karimi, Z., Dashti, S., Porter, K., Liel, A., & Franke, K. (2018). A Physics-Informed Semi-Empirical Probabilistic Model for the Settlement of Shallow-Founded Structures on Liquefiable Ground. *Geotechnique*. [https://doi.org/10.1680/jgeot.17.P.174].
17. Burland, J. B., and Wroth, C. P. (1974). "Settlement of buildings and associated damage." Proc, Conf. on Settlement of Structures, Pentech Press, London, England, 611–654.
18. Burland, J. B., and Broms, B. B., and de Mello, V. F. B. (1977). "Behavior of foundations and structures." State-of-the-Art Report. Proc, 9thInt'l. Conf. on Soil Mech. and Found. Engr., II, Tokyo, Japan, 495–546.
19. Campbell, K. W., and Bozorgnia, Y. 2011. Predictive equations for thehorizontal component of standardized cumulative absolute velocityas adapted for use in the shutdownof U.S. nuclear power plants,Nucl. Eng. Des. 241, 2558–2569.
20. Castiglia, M., Fierro, T., Santucci de Magistris, F. (2020). Pipeline Performances under Earthquake-Induced Soil Liquefaction: State of the Art on Real Observations, Model Tests, and Numerical Simulations. Shock and Vibration, 10.1155/2020/8874200.
21. CEN 2017a: prEN 1997-1, Eurocode 7: Geotechnical design.
22. Cetin, K. O., Youd, T.L., Seed, R.B. Bray, J. D., Sancio, R., Lettis, W., Tolga Yilmaz, M., H.Turan Durgunoglu (2002). Liquefaction-induced ground deformations at Hotel Sapanca during Kocaeli (Izmit),Turkey earthquake, Soil Dynamics and Earthquake Engineering, Volume 22, Issues 9–12, 2002, Pages 1083–1092, ISSN 0267–7261, https://doi.org/10.1016/S0267-7261(02)00134-3.
23. Chiaradonna, A., Lirer, S., Flora, A. (2020). A liquefaction potential integral index based on pore pressure build-up. Engineering Geology, Vol. 272. 10.1016/j.enggeo.2020.105620
24. Chung, R. (1996), January 17, 1995 Hyogoken-Nanbu (Kobe) Earthquake: Performance of Structures, Lifelines, and Fire Protection Systems (NIST SP 901), Special Publication (NIST SP), National Institute of Standards and Technology, Gaithersburg, MD, [online], https://doi.org/10.6028/NIST.SP.901
25. CSAPEISLA (2016) State of the Art and Practice in the Assessment of Earthquake-Induced Soil Liquefaction and Its Consequences, Report of the Committee on State of the Art and Practice in Earthquake Induced Soil Liquefaction Assessment; Board on Earth Sciences and Resources; Division on Earth and Life Studies; National Academies of Sciences, Engineering, and Medicine, ISBN: 978-0-309-44027-1
26. Cubrinovski, M., J. D. Bray, M. Taylor, S. Giorgini, B. A. Bradley, L. Wotherspoon, and J. Zupan. 2011b. "Soil liquefaction effects in the central business district during the February 2011 Christchurch earthquake." Seismol. Res. Lett. 82 (6): 893–904.
27. Cubrinovski, M., van Ballegooy, S. (2017) System response of liquefiable deposits. In: 3rd International conference on performance based design in earthquake geotechnical engineering
28. Dafalias, Y.F., Manzari, M.T. (2004). Simple plasticity sand model accounting for fabric change effects. J. Eng. Mech. 130(6), 622–634.
29. Daniell, J.E. and Vervaeck, A. (2012). The CATDAT Damaging Earthquakes Database – 2011 – Year in Review. CEDIM Research Report 2012-01, Karlsruhe, Germany.
30. Dashti, S., Bray, J.D. (2013) Numerical simulation of building response on liquefiable sand. J Geotech Geoenviron Eng ASCE 139(8):1235–1249
31. Facciorusso, J., Madiai, C., and Vannucchi, G. (2016). The 2012 Emilia earthquake (Italy): geotechnical characterization and ground response analyses of the paleo-Reno river levees. Soil Dynamics and Earthquake Engineering, 86, 71–88.
32. Fisher R. A. (1918). The correlation between relatives on the supposition of mendelian inheritance. Trans. R. Soc. Edinb. 53: 399–433.

33. Fioravante, V., Giretti, D., Abate, G., Aversa, S., Boldini, D., Capilleri, P. P. and Facciorusso, J. (2013). Earthquake geotechnical engineering aspects of the 2012 Emilia-Romagna earthquake (Italy).
34. Flora, A., Bilotta, E., Chiaradonna, A. *et al.* (2021). A field trial to test the efficiency of induced partial saturation and horizontal drains to mitigate the susceptibility of soils to liquefaction. *Bull Earthquake Eng* 19, 3835–3864 https://doi.org/10.1007/s10518-020-00914-z
35. Fotopoulou, S., Karafagka, S., Pitilakis K. (2018). Vulnerability assessment of low-code reinforced concrete frame buildings subjected to liquefaction-induced differential displacements. Soil Dynamics and Earthquake Engineering 110, 173–184.
36. Grant, R., Christian, J.T., and Vanmarcke, E.H. 1974. "Differential settlement of buildings". Journal of Geotechnical Engineering Division, ASCE, 100(9), pp. 973–991.
37. Ishihara, K., (1996) Soil behaviour in earthquake geotechnics. Oxford University Press Inc, New York, NY
38. Ishihara, K., and M. Yoshimine. 1992. "Evaluation of settlements in sand deposits following liquefaction during earthquakes." Soils Found. 32 (1): 173–188. https://doi.org/10.3208/sandf1972.32.173.
39. Ishii, Y., Tokimatsu, K. (1988) Simplified procedures for the evaluation of settlements of structures during earthquakes. In: Proceedings from the ninth world conference on earthquake engineering, Tokyo-Kyoto, Japan, vol 3, pp 95–100
40. Itasca Consulting Group, Inc. (2016). FLAC - Fast Lagrangian Analysis of Continua, Ver. 8.0. Minneapolis: Itasca.
41. Iwasaki, T., Tatsuoka, F., Tokida, K., and Yasuda, S., (1978), "A Practical Method for Assessing Soil Liquefaction Potential Based on Case Studies at Various Sites in Japan", 2nd International Conference on Microzonation for Safer Construction Research and Application, pp. 885–896.
42. Karamitros. D.K., Bouckovalas. G.D., Chaloulos. Y.K. (2013):"Seismic settlements of shallow foundations on liquefiable soil with a clay crust". Soil Dynamics and Earthquake Engineering. 46. 64–76.
43. Karamitros. D.K., Bouckovalas. G.D., Chaloulos. Y.K. (2013):"Insight into the Seismic Liquefaction Performance of Shallow Foundations". Journal of Geotechnical and Geoenvironmental Engineering 139(4):599–607 10.1061/(ASCE)GT.1943-5606.0000797
44. Karimi, Z., Dashti, S., Bullock, Z., Porter, K., Liel, A. (2018). Key predictors of structure settlement on liquefiable ground: a numerical parametric study, Soil Dynamics and Earthquake Engineering, Volume 113, 2018, Pages 286–308, ISSN 0267–7261, https://doi.org/10.1016/j.soildyn.2018.03.001.
45. Kuhleimeyer, R., & Lysmer, J. (1973). Finite element method accuracy for wave propagation problems. Journal of the soil mechanics and foundations division, ASCE, 99(SM5), 421–427.
46. Luque, R., and J. Bray. 2015. "Dynamic analysis of a shallow-founded building in Christchurch during the Canterbury earthquake sequence." In Proc., 6th Int. Conf. on Earthquake Geotechnical Engineering. Christchurch, New Zealand.
47. Luque, R., and J. Bray. 2017. "Dynamic analyses of two buildings founded on liquefiable soils during the Canterbury earthquake sequence." J. Geotech. Geoenviron. Eng. 143 (9): 04017067. https://doi.org/10.1061/(ASCE)GT.1943-5606.0001736.
48. Luzi, L., Pacor, F., Puglia, R. (2019). Italian Accelerometric Archive v3.0. Istituto Nazionale di Geofisica e Vulcanologia, Dipartimento della Protezione Civile Nazionale. doi: 10.13127/itaca.3.0
49. Macaulay, T. (2009). Critical infrastructures. Taylor & Francis, Abingdon
50. Mazzolani F.M. (1967). La progettazione delle travi di fondazione su suolo alla Winkler. RIG, vol. I, n. 4bis.
51. McCulloch, W., & Pitts, W. (1943). A logical calculus of ideas immanent in nervous activity. Bulletin of Mathematical Biophysics, 5(4), 115–133. https://doi.org/10.1007/BF02478259
52. Meyerhof, G. G. (1953). "Some recent foundation research and its application to design." Struct. Engr., 31, 151–167.
53. Paolella, L., Spacagna, R.L., Chiaro, G. et al. (2021). A simplified vulnerability model for the extensive liquefaction risk assessment of buildings. Bull Earthquake Eng 19, 3933–3961. https://doi.org/10.1007/s10518-020-00911-2
54. Polshin, D. E., and Tokar, R. A. (1957). "Maximum allowable non-uniform settlement of structures." Proc, 4th Inl. Conf. on Soil Mech. and Found. Engr., 1, London, England, 402–405.
55. Poulos, H.G. (2001). Pile foundations. Ch. 10 of Geotechnical and Geoenvironmental Handbook, Ed. R.K. Rowe, Kluwer Academic Publishers, Boston, 261–304. Foundations and retaining structures - Research and practice.
56. Salvatore, E., Modoni, G., Mascolo, M.C., Grassi, D., Spagnoli, G. (2020). Experimental Evidence of the Effectiveness and Applicability of Colloidal Nanosilica Grouting for Liquefaction Mitigation. Journal of Geotechnical and Geoenvironmental Engineering. 146. 04020108. 10.1061/(ASCE)GT.1943-5606.0002346.
57. Seed, R.B., Cetin, K.O., Moss, R.E.S., Kammerer, A., Wu, J., Pestana, J., Riemer, M., Sancio, R.B., Bray, J.D., Kayen, R.E., Faris, A. (2003) Recent advances in soil liquefaction engineering: a unified and consistent framework. Keynote presentation, 26th Annual ASCE Los Angeles Geotechnical Spring Seminar, Long Beach, CA, April 30
58. Sherif, G. and Koenig, G. (1975). Rafts and beams on compressible subsoil. Tables for calculation of soil pressure, settlement, shear forces and moments according to the modulus of compressibility-method. Springer-Verlag.
59. Sinatra, L., and Foti, S. (2015). The role of aftershocks in the liquefaction phenomena caused by the Emilia 2012 seismic sequence. Soil Dynamics and Earthquake Engineering, 75, 234–245.
60. Skempton, A. W., and MacDonald, D. H. (1956). "The allowable settlement of buildings." Proc, Inst, of Civ. Engrs., Part III, 5, 727–784.

61. Tokimatsu, K., and H. B. Seed. 1987. “Evaluation of settlements in sands due to earthquake shaking.” J. Geotech. Eng. 113 (8): 861–878. https://doi.org/10.1061/(ASCE)0733-9410(1987)113:8(861).
62. van Ballegooy, S., Malan, P., Lacrosse., V., Jacka, M.E., Cubrinovski, M., Bray, J.D., O’Rourke, T.D., Crawford, SA, and Cowan, H. 2014a. Assessment of liquefaction-induced land damage for residential Christchurch, Earthquake Spectra, 30(1): 31–55.
63. Wahls, H. E. (1981). "Tolerable settlement of buildings." J. Geotech. Engrg., ASCE, 107(11), 1489–1504.
64. Yasuda S., Harada K., Ishikawa, K., Kanemaru, Y. (2012) Characteristics of Liquefaction in Tokyo Bay Area by the 2011 Great East Japan Earthquake. Soils Found 52:793–810
65. Yoshida, N., Tokimatsu, K., Yasuda, S., Kokusho, T., and Okimura, T. (2001). “Geotechnical aspects of damage in Adapazari city during 1999 Kocaeli, Turkey earthquake.” Soils Foundation., 41(4), 25–45.
66. Youd, T.L. and Hoose, S.N. (1978), "Historic Ground Failures in Northern California Associated with Earthquakes", Professional Paper 993, U.S. Geological Survey.
67. Youd TL et al (2001) Liquefaction resistance of soils: Summary report from the 1996 NCEER and 1998 NCEER/NSF workshops on evaluation of liquefaction resistance of soils. J Geotech Geoenviron Eng 127(10):817–833

Figures

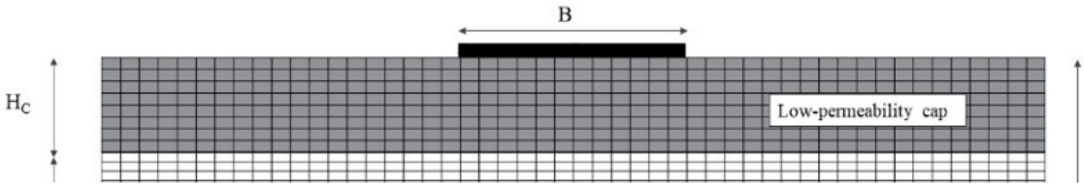

Figure 1

Layout of the implemented numerical model.

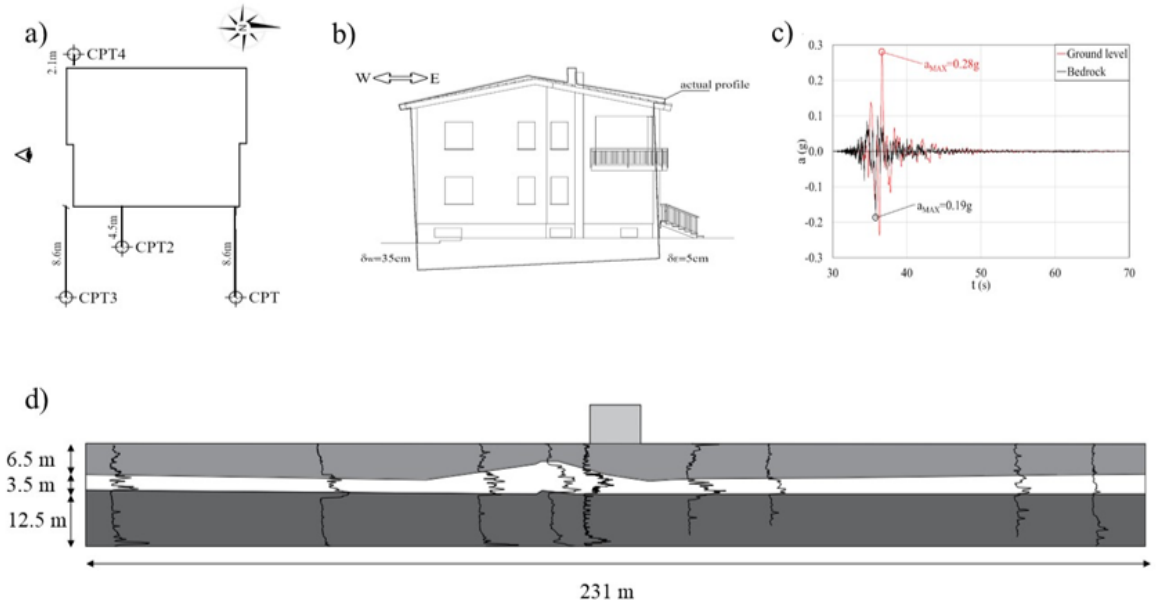

Figure 2

Building's plan and closest CPT tests (a), settlement profile (b), acceleration time history (c) and subsoil profile (d) of the selected case study.

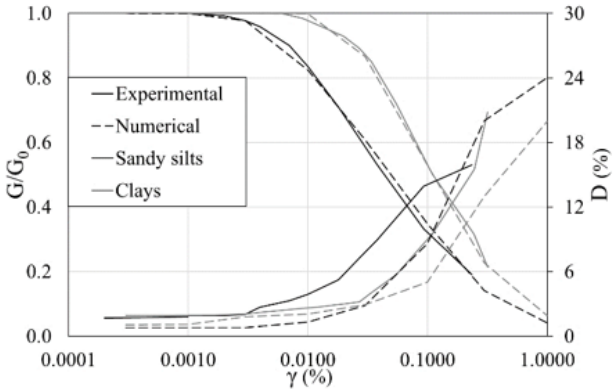

Figure 3

Shear modulus degradation and damping curves numerically and experimentally obtained for the different subsoil layers (clays represent the upper and lower layers, sandy silts represent the intermediate layer).

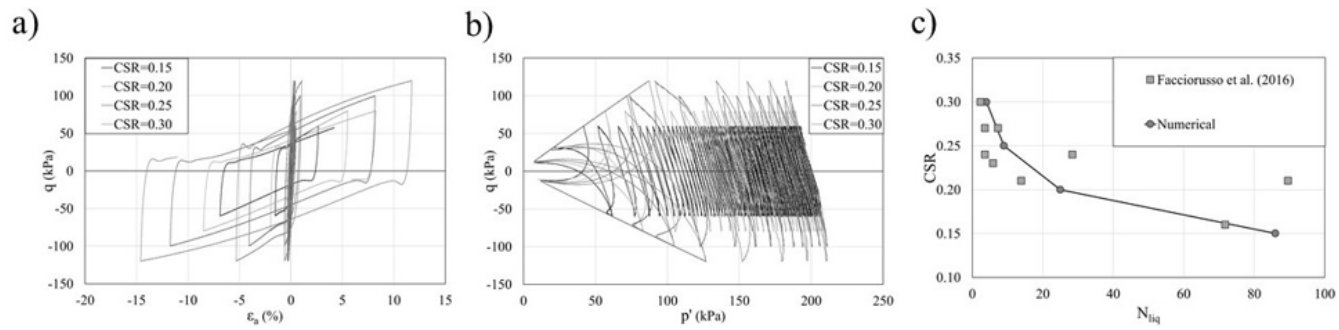

Figure 4

Results of the numerical liquefaction tests in terms of a) deviatoric stress against axial strain curves; b) deviatoric stress against main effective stress curves; c) liquefaction curves.

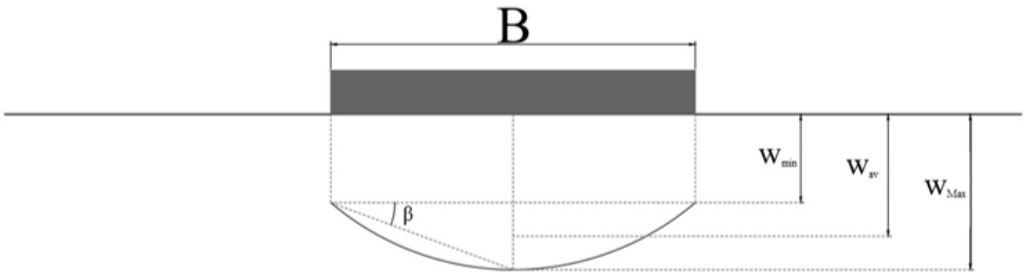

Figure 5

Typical output and definition of the characteristic variables.

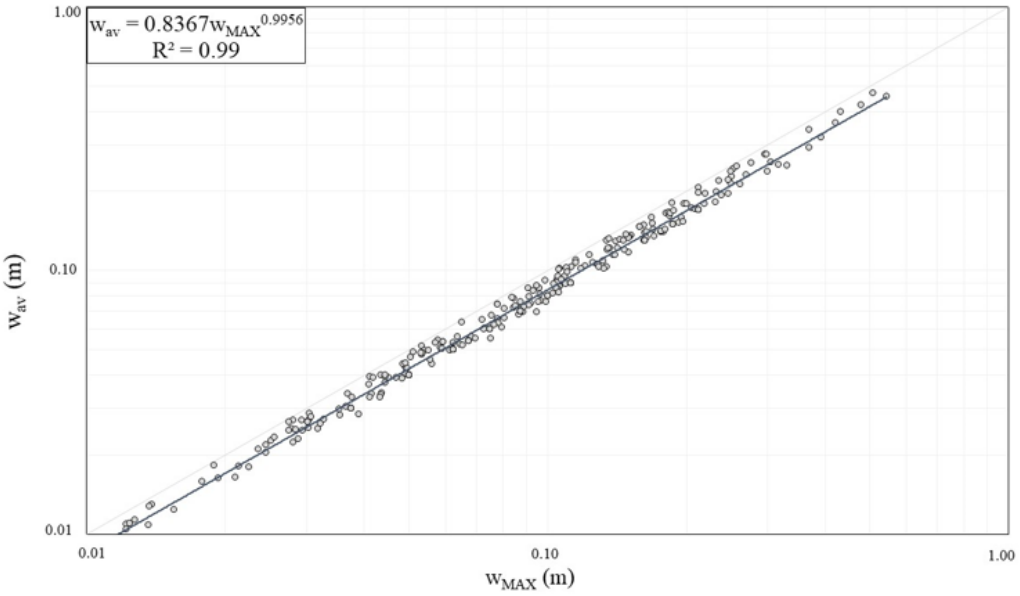

Figure 6

Absolute versus mean settlement obtained in all numerical analyses.

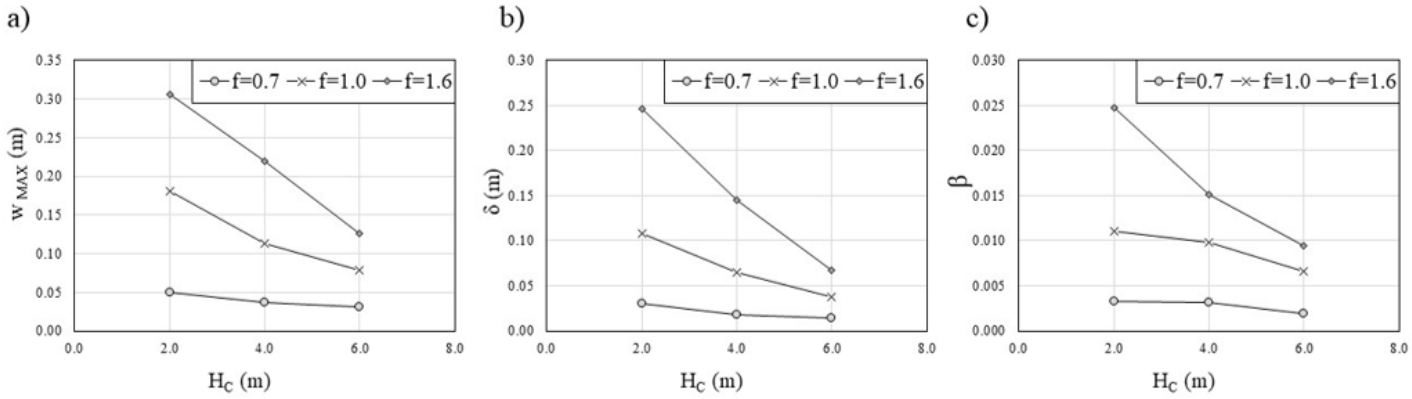

Figure 7

Absolute settlement (a), differential settlement (b), and angular distortion (c) for variable thicknesses of the crustal layer (H_C) (calculation has been performed assigning the Emilia Romagna earthquake, H_L=6m, Dr=40%, s_u=50kPa B=10m, q=50kPa, EI=0 MN*m).

Figure 8

Absolute settlement (a), differential settlement (b), and angular distortion (c) for variable undrained shear strength (s_u) of the crust (calculation has been performed assigning the Emilia Romagna earthquake, H_L=6m, H_C =4m, D_r=40%, B=10m, q=50kPa, EI=0 MN*m).

Figure 9

Absolute settlement (a), differential settlement (b), and angular distortion (c) for variable thickness of liquefiable layer (H_L) (calculation has been performed assigning the Emilia Romagna earthquake, H_C =4m, Dr=40%, s_u=50kPa, B=10m, q=50kPa, EI=0 MN*m).

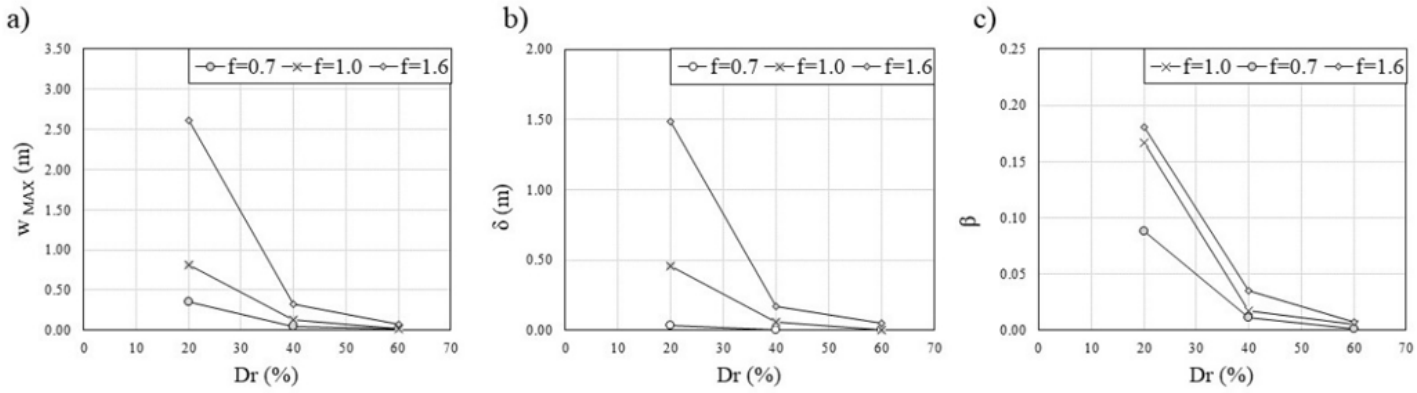

Figure 10

Absolute settlement (a), differential settlement (b), and angular distortion (c) for variable relative density (D_r) (calculation has been performed assigning the Emilia Romagna earthquake, H_L=6m, H_C =4m, s_u=50kPa, B=10m, q=50kPa, EI=0 MN*m).

Figure 11

Absolute settlement (a), differential settlement (b), and angular distortion (c) for variable relative foundation width (B) (calculation has been performed assigning the Emilia Romagna earthquake, H_L=6m, H_C =4m, D_r=40%, s_u=50kPa, q=50kPa, EI=0 MN*m).

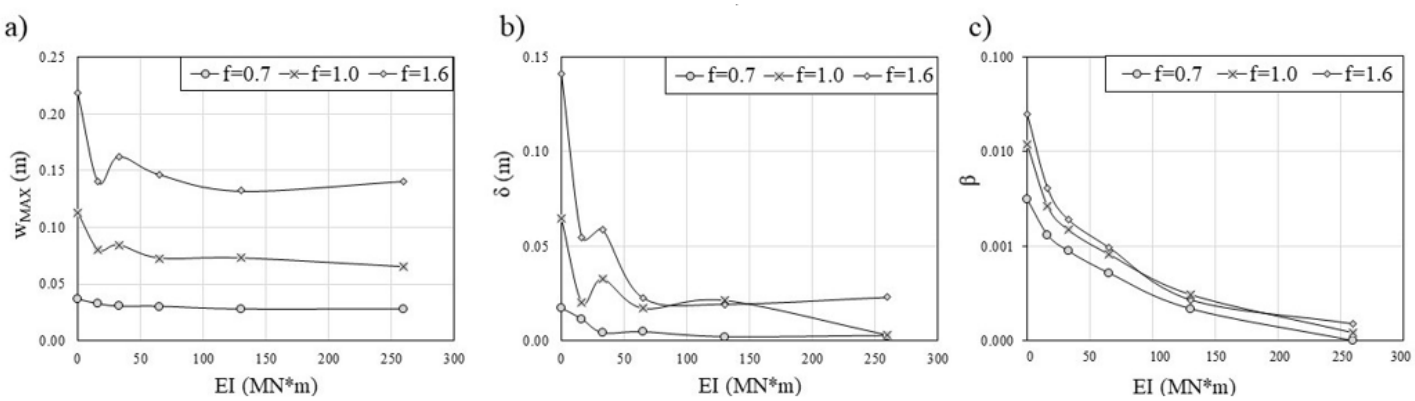

Figure 12

Absolute settlement (a), differential settlement (b), and angular distortion (c) for variable stiffness (EI) (calculation has been performed assigning the Emilia Romagna earthquake, H_L=6m, H_C =4m, D_r=40%, s_u=50kPa, q=50kPa, B=10).

Figure 13

Effect of superstructure in terms of ratio between foundation movements computed with the model contemplating superstructure inertia and the corresponding results of the basic analysis (ρ) (a); plot box of effect of H/B ratio for each foundation movement.

Figure 14

Mean settlements predicted with the numerical calculation vs median settlements computed with the Bullock *et al.* (2018) semi-empirical method.

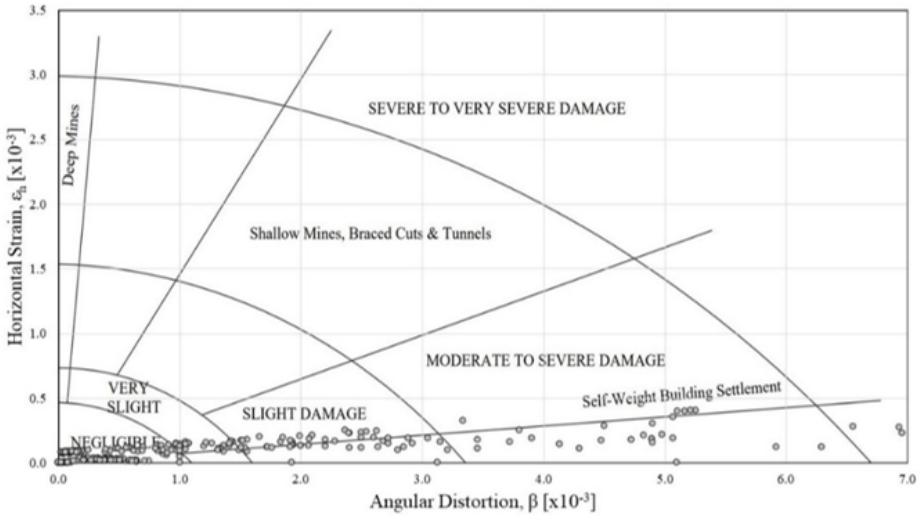

Figure 15

Key evidence from the parametric study: ground horizontal strain vs angular distortion overlapped to the plot of Boscardin and Cording (1989).

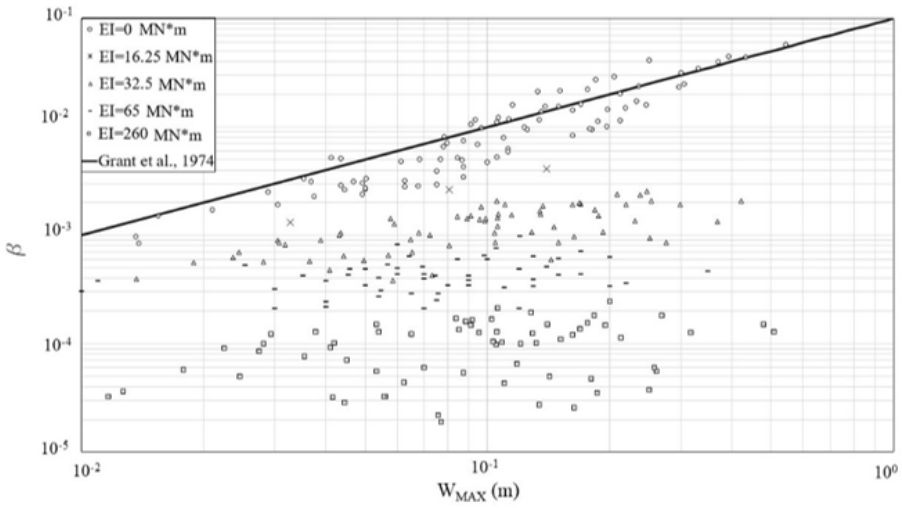

Figure 16

Angular distortion vs maximum absolute settlement overlapped to the plot of Grant *et al.* (1974).

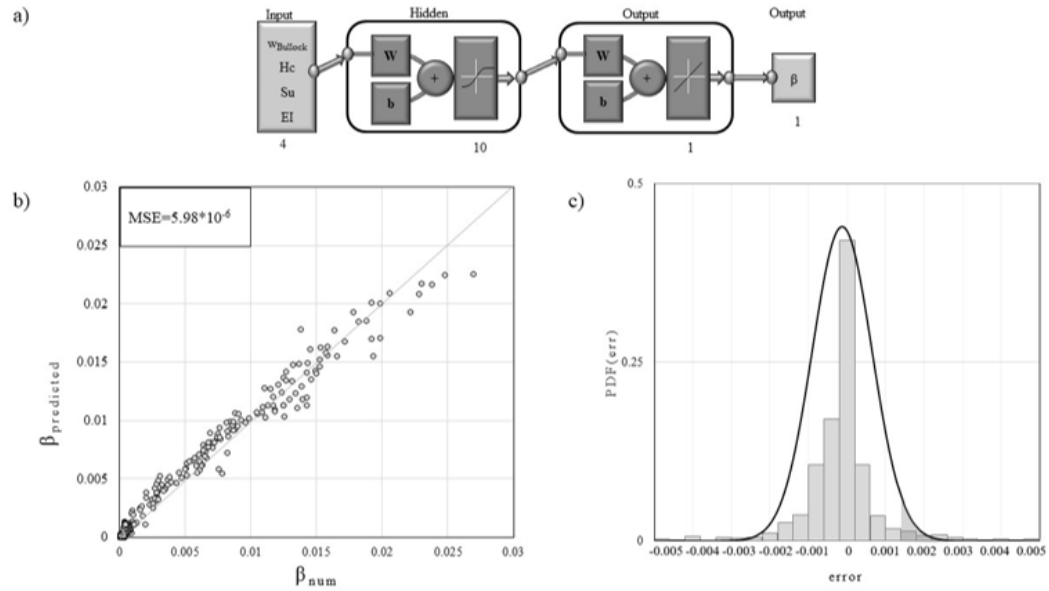

Figure 17

Structure of the artificial neural network (a), regression (b), statistical analysis and frequency distribution of error (c).

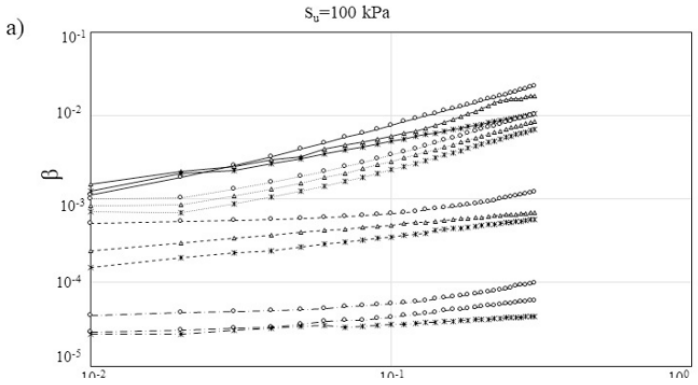

Figure 18

Example of b prediction with ANN.